Electronic structure and equation of state data of warm dense gold

P. Renaudin,* V. Recoules, P. Noiret, and J. Clérouin
Département de Physique Théorique et Appliquée, CEA/DAM Île-de-France, BP12, 91680 Bruyères-le-Châtel Cedex, France
(Received 7 October 2005; published 16 May 2006)

Equation of state data and electrical resistivity of warm dense gold were measured in the internal energy range 8–12 MJ/kg. Experimental results were compared with quantum molecular dynamics simulations. The theoretical results match well the experimental data, allowing a detailed interpretation of the theoretical thermodynamic properties and frequency-dependent conductivities.

DOI: 10.1103/PhysRevE.73.056403 PACS number(s): 52.50.Nr, 52.65.Yy, 52.25.Fi, 52.25.Kn

I. INTRODUCTION

There has been a growing interest in the exploration of atomic properties of strongly coupled partially degenerate plasmas, also referred to as warm dense matter (WDM). This complex thermodynamic regime, encountered in Jovian planets' interior, cool dense stars, and in laboratory experiments, opens a challenging field for both experiments and theoretical calculations [1]. However, at the present stage, experimental data are scarce and there are a very small number of *ab initio* theories that can reproduce thermodynamic data and transport coefficients of such plasmas in a self-consistent way [2–5].

From the theoretical point of view, the calculations are made using various assumptions about electronic or ionic structure. These two quantities are difficult to obtain, especially in the WDM regime where a self-consistent description of the ionic and electronic structure is needed to obtain an accurate description of the atomic properties. It is especially true when electron localization and/or details of the ionic structure can play an important role, particularly in the vicinity of a metal-insulator transition. Moreover, the frequency-dependent part of the conductivity remains excessively hard to calculate, especially when the frequency-dependent conductivity shows no Drude character at low frequencies.

From the experimental point of view, the interest in WDM studies is mainly motivated by laboratory experiments involving short-pulsed lasers or exploded wire experiments. Some experiments have been carried out to measure the electrical resistivity [6,7], the optical properties [8–12], the ionization and recombination dynamics of transient plasmas [13], or the combination of electrical resistivity and equation of state (EOS) data [14,15] under conditions of thermal equilibrium and at sufficiently high pressure to be well above the predicted critical point pressure.

Due to its chemical inertness, large isothermal compressibility, and the large pressure and temperature stability ranges of its ambient fcc phase, gold has been employed as a primary EOS for many years [16]. However, noble metals as gold present a complex electronic structure and provide a well-known challenge for theoretical modeling. Recent measurements of electrical conductivity of solid density gold have been reported in the internal energy range 0.2–20 MJ/kg [12]. In this study, collision time and electron density were inferred using the Drude model [17].

In this paper, we report on combined electrical resistivity, pressure, and internal energy variation measurements of a gold plasma at a density of 0.5 g/cm^3. Compared to the experimental works previously reported, the achieved density studies a thermodynamic regime particularly interesting because it maps the transition between the low-density atomic vapor and the partially ionized plasma. The experiments were performed in an isochoric plasma closed vessel (EPI) where a sample goes from the solid state at normal density and room temperature to a well-known density plasma regime in the internal energy range 8–12 MJ/kg.

The goal of this paper is to show, by a careful comparison with experimental data, that quantum molecular dynamics simulations are particularly well suited for describing this regime and are providing a consistent view of the system in terms of the EOS and the transport properties, even for a noble metal which presents a complex electronic structure.

This paper is organized as follows. In Sec. II, we will describe the experimental setup. Details of theoretical calculations are given in Sec. III. Experimental and theoretical results are presented in Sec. IV. Section V is the conclusion.

II. EXPERIMENTAL SETUP

The experiments were performed in EPI, which has been described in detail in previous papers [14,15]. EPI combines two techniques: a high-pulse power bank to obtain a fast heating of the metallic sample and a high-pressure closed vessel built in sapphire that mechanically controls the plasma volume. The sapphire rings are bound in the center of high-pressure tungsten carbide rings forming (once stacked) a tube of 19 cm in length and 1.2 cm in diameter. This facility allows an absolute measurement of the internal energy, pressure, and electrical resistance. Seven gold tubes with a length of 19 cm, an outside diameter of 1 mm, an inside diameter of 0.7 mm, and a purity of 99.95% are linked together with a 500 μm thick gold wire and placed inside the vessel. The amount of matter in the chamber yields the exact density of the homogeneous plasma phase. For the described experiments, a total gold mass of 10.8 g leads to an average density of 0.5 g/cm^3. Current is driven from four capacitors con-

*Electronic address: patrick.renaudin@cea.fr

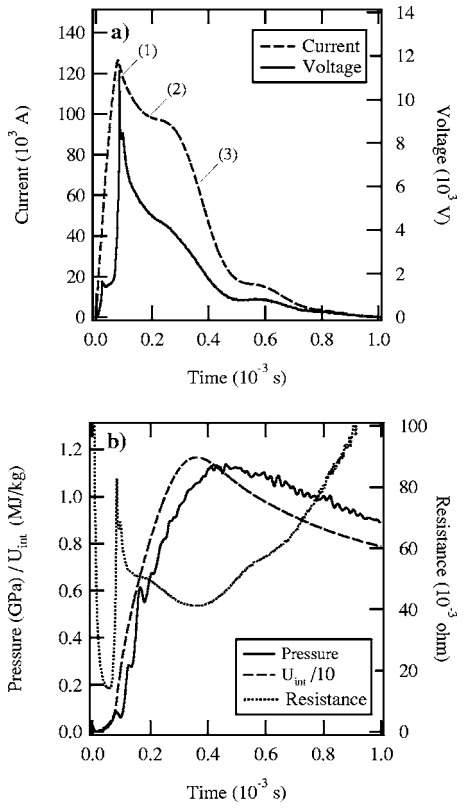

FIG. 1. Time evolution of (a) the current and the voltage and (b) the pressure, the internal energy U_{int}, and the electrical resistance measured during the experiment. The homogeneous density of gold is equal to 0.5 g/cm^3.

nected in parallel, totaling 2.42 mF, and is switched by a pressurized spark gap switch. Internal inductance of the circuit is 6 μH. With such setup, the sample is heated in 100 microseconds. A Rogowski belt surrounds one electrode to measure the time derivative of the current, and a resistive divider is used to measure the voltage drop across the plasma. The time derivative dI/dt of the current and the inductance L of the plasma are small enough to make the $L \times dI/dt$ term negligible compared to the measured voltage, except at the very beginning of the discharge. Therefore, no inductive correction is needed to obtain the plasma resistivity from the current and voltage measurements [shown in Fig. 1(a)] [14]. Two acceleration-compensated piezoelectrical sensors with 2 μs rise time are placed at each end of the vessel to measure the pressure during the discharge, allowing a maximum pressure measurement of 2.5 GPa. The time evolution of the pressure, the internal energy, and the electrical resistance measured during one experiment are reported in Fig. 1(b). The plotted pressure is the mean value of the two pressures measured at each end of the vessel. These two pressures are equal within 2%. The calibration procedure produces a 15% uncertainty in the pressure of the plasma [15]. During the evaporation, the liquid and the vapor are heated independently. At the point labeled (1) in Fig. 1(a), the effective phase of vaporization begins. At that time, the pressure rises quickly. The heating becomes isochoric when the vapor ionization induces an arc regime. No arc regime was observed during these experiments and we assumed that homogeneity was achieved at the point labeled (2), when an inflection point appears on the current curve. At the point (3) (at time 350 μs), the maximum of the electrical conductivity is reached. Beyond point (3), cooling begins. Finally, the interpretation of the resistance $R(t)$ in term of resistivity $\rho(t)$ is meaningful only when the plasma is homogeneous, i.e., between points (2) and (3). The input energy and the electrical resistivity of the plasma are inferred from the current and voltage measurements [14]. Note that all quantities are known versus the internal energy variation. To preserve the quality of our data we will show them this way. The uncertainties in the measurements of the conductivity and the internal energy variation are related to the accuracy of current and voltage measurements and are estimated at about 15%.

III. THEORETICAL CALCULATIONS

In quantum molecular dynamics (QMD), the ions follow classical trajectories determined by the forces acting on them while the electronic subsystem remains in ground state at each instant (the Born-Oppenheimer principle). The equations of motions for the ions are solved via the velocity Verlet algorithm. The forces are calculated from the electronic ground state using the Hellman-Feynmam theorem. For each position of the ions, the ground-state electronic density is computed by minimizing the free-energy functional of the electron gas in the framework of finite temperature density functional theory [18]. This leads to solution of a set of equations for the electronic orbitals ψ_n and eigenvalues ϵ_n of the Kohn-Sham form,

$$\left[-\frac{1}{2}\nabla^2 + V_{\text{ion}}(r) + V_H(r) + V_{xc}(r)\right]\psi_n(r) = \epsilon_n \psi_n(r), \quad (1)$$

where the first term is the kinetic energy of a system of noninteracting electrons with density ρ, V_{ion} is the electron-ion potential, V_H is the Hartree potential, V_{xc} is the exchange and correlation potential. In this work, the exchange and correlation term in the density functional expression is represented by the local density approximation. It is expressed from the exchange and correlation energy of a uniform electron gas with the same electronic density as the one of the system. We used the energy estimation computed by Ceperley and Adler using a Monte Carlo method [19]. The projector augmented wave (PAW) method is used to construct electron-ion potential [20,21]. Only valence electrons are explicitly represented. The Au 5*d* and 6*s* electrons are counted as valence electrons, and all more tightly bond electrons are counted as part of the core. The valence electronic orbitals are expanded in plane waves. In this expansion, all plane waves are included whose wave vector $\mathbf{G}$ satisfies $\hbar^2\mathbf{G}^2/2m < E_{\text{cut}}$, where E_{cut} is referred to as the plane-wave cutoff energy. The calculations are taken to convergence by using an energy cutoff of 287 eV.

As a test for the potential transferability, we compute some properties of solid gold and of the dimer Au_2 at zero pressure and zero temperature. For the lattice constant and bulk modulus of solid gold, Brillouin zone sampling is performed by the usual Monkhorst-Pack scheme [22] and we use 120 k points. This method generate a set of special k

points in the Brillouin zone which provides an efficient means of integrating periodic functions. We obtain, respectively, 4.08 Å and 183 GPa to be compared with experimental values of 4.08 Å and 172 GPa [23]. According to Boettger's result, we found that the local density approximation gives better static lattice properties than the generalized gradient approximation [24,25] for solid gold. For the dimer, we compute an equilibrium distance of 2.47 Å. The experimental value is 2.47 Å [26]. These results are comparable to those obtained using all-electron density functional calculations [23,27].

QMD simulations for warm dense gold are performed for six temperatures ranging from 15 000 to 40 000 K. A 16-atom cubic cell of appropriate size to reproduce the experimental density $\rho=0.5$ g/cm^3 is used with periodic boundary conditions of the simple cubic type. Electronic orbitals are populated according to the Fermi-Dirac distribution function, with a number of states from 1000 to 1500 and the electronic temperature set equal to that of ions. Trajectories are generated in the microcanonical ensemble for 500 time steps of 2 fs. In this ensemble, the system remains free to adjust to an average equilibrium ionic temperature, and the total energy should be conserved. During the molecular dynamic simulation, the Γ point only is used to sample the Brillouin zone. Then, we use four k vectors to obtain the detailed electronic structure needed to compute optical response of warm dense gold. For all simulations, we use the VASP (Vienna *ab initio* Simulation Program) plane-wave code developed at the Technical University of Vienna [28].

In linear response theory, the real part of the frequency-dependent conductivity is given in terms of the Kubo-Greenwood equation [29,30],

$$\sigma(\omega) = \frac{2\pi e^2}{3\omega} \int d\boldsymbol{k} \sum_{n,m} (f_n - f_m) \times |\langle \psi_n | \hat{\boldsymbol{v}} | \psi_m \rangle|^2 \delta(E_m - E_n - \hbar\omega), \quad (2)$$

where ω is the frequency, e is the electronic charge, ψ_n and E_n are the electronic eigenstates and eigenvalues for the electronic state n, f_n is the Fermi-Dirac distribution function, and $\hat{\boldsymbol{v}}$ is the velocity operator. We use a Gaussian broadening of the δ function with a width set to obtain smooth and converged curves. Following the QMD simulations, six configurations were extracted from the calculated trajectories. For each configuration, the frequency-dependent conductivity was calculated using the Kubo-Greenwood formulation.

A QMD simulation of the fcc solid phase at 300 K with 108 atoms sets the reference energy. All further energies are given relative to this reference energy, allowing a direct comparison between theoretical results and experimental data.

IV. DISCUSSION

The experimental and QMD pressures are reported in Fig. 2(a). The experimental electrical resistivity is compared with QMD results in Fig. 2(b). All the experimental data are reported in Table I.

The interpretation of the resistance in terms of resistivity and the calculation of the internal energy from the input energy are meaningful only between points (2) and (3) in Fig. 1(a). Therefore, the experimental data are plotted from 80 to 11.5 MJ/kg, corresponding to the evolution of the internal energy between these two points. Determining the timing when the plasma homogeneity is reached, i.e., measuring the saturation pressure and/or the electrical resistivity on the

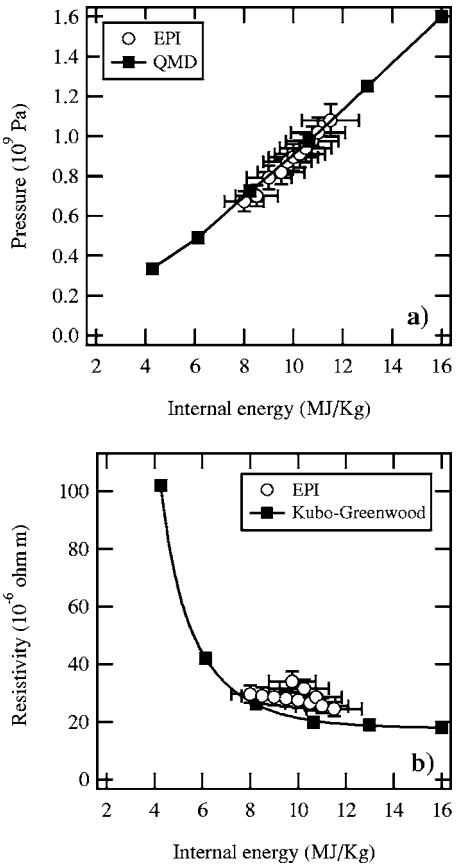

FIG. 2. Experimental and theoretical (a) pressure and (b) electrical resistivity versus internal energy variation for gold at $\rho=0.5$ g/cm^3. Each black square is a QMD calculation corresponding to the four considered temperatures and the line is for readability.

TABLE I. Experimental internal energy U_{int}, electrical resistivity ρ_e, and pressure P of gold at 0.5 g/cm^3.

U_{int} (MJ/kg)	ρ_e (Ω m)	P (GPa)
8.00	2.95×10^{-5}	0.672
8.50	2.90×10^{-5}	0.700
9.00	2.85×10^{-5}	0.792
9.50	2.80×10^{-5}	0.820
9.75	3.40×10^{-5}	0.871
10.00	2.75×10^{-5}	0.895
10.25	3.15×10^{-5}	0.910
10.50	2.65×10^{-5}	0.940
10.75	2.85×10^{-5}	0.975
11.00	2.55×10^{-5}	1.017
11.50	2.45×10^{-5}	1.080

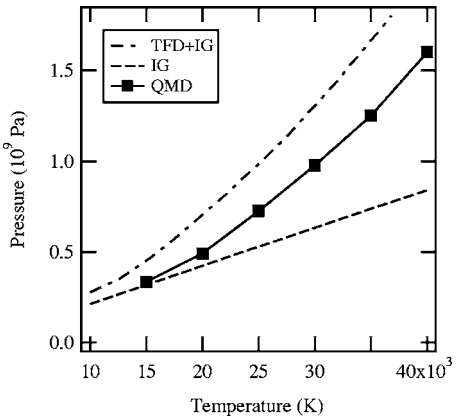

FIG. 3. Pressure of gold at a density of $\rho=0.5$ g/cm^3 as a function of temperature, calculated with different theoretical models. Each black square is a QMD calculation and the line is for readability.

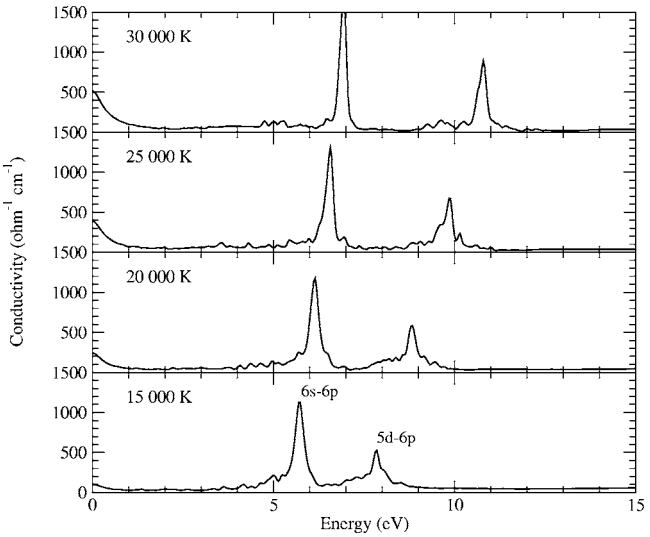

FIG. 4. Frequency-dependent conductivity for gold at $\rho=0.5$ g/cm^3 and for temperatures from 15 000 to 30 000 K.

saturation curve, would present a new opportunity to test EOS and transport theories along the saturation curve and in the vicinity of a metal-insulator transition [7]. Such work is beyond the scope of this study.

The QMD pressures agree perfectly with experimental results. This excellent agreement demonstrates that the QMD describes very accurately the fluid and also the various density effects in the thermodynamic regime of the experiment. In various atomic models, density effects such as pressure ionization and plasma ion correlation are entered through the ion sphere model or in a more phenomenological way, in contrast with QMD calculations. We show in Fig. 3 the considered gold isochore calculated using the QMD, the Thomas-Fermi-Dirac (TFD) model, and the ideal gas (IG) model. At low temperatures, the ionization effects are negligible and the thermodynamic properties of the fluid calculated by QMD are those of an ideal gas. For the temperature range considered, the main contribution to the pressure is the ionic contribution which represents more than 95% of the total pressure at 10 000 K and 65% at 30 000 K. The sum of the TFD electronic pressure and the IG ionic pressure, noted as TFD+IG in Fig. 3, is 30% higher than the VASP pressure. The Thomas-Fermi and TFD models overestimate the electronic pressure in this low-temperature and intermediate density regime. This comparison shows that, for the highest temperatures displayed in Fig. 3, the accuracy of the EOS models depends on their capabilities to accurately describe the electronic structure. The excellent agreement between experimental EOS data and QMD simulations shows that the calculated electronic structure is well representative of warm dense gold. To further quantify the modification of the electronic structure of gold as temperature is varied, we now consider the variation of the resistivity over the same physical conditions, as displayed in Fig. 2(b).

The QMD electrical resistivities agree well with the experimental data. This good agreement shows that the Kubo-Greenwood formulation of the electrical conductivity is accurate for the warm dense noble metals. We now consider the whole optical conductivity as given by the Kubo-Greenwood formula. The evolution of the frequency-dependent conductivity of gold with temperature is reported in Fig. 4.

As for simple [4,31] and transition [32] metals in the same thermodynamic regime, the frequency-dependent conductivity is the sum of interband transitions (the two major peaks located between 5 and 11 eV), and intraband transitions with a Drude form at low frequencies. At $T=15\,000$ K, the free-free transitions at low frequency are very weak. This is consistent with the fact that gold is nearly an ideal gas at this low temperature and, hence, becomes an insulator. Considering the $5d$ and $6s$ orbitals and the absence of f orbital in the PAW potential used here, two allowed atomic transitions exist in the calculated spectral range: the $6s\rightarrow 6p$ and $5d\rightarrow 6p$ transitions. Therefore, the two major peaks in Fig. 4, around 5.7 and 7.8 eV for the smallest temperature, can be attributed to these two transitions, respectively. One limitation of the plane-wave technique is that this nonlocal basis set does not provide a natural way of quantifying local atomic properties. Moreover, the density functional theory, which considers statistically populated levels, realizes a continuous transition from the atomic to the singly ionized state and, hence, a continuous shift of the energy of the different transitions. At $T=30\,000$ K, the Drude form at low frequencies is more pronounced, in accordance with the fact that the number of free electrons and the population of Au^+ have increased.

We now examine the implications of the results by assuming nearly free electron (NFE) behavior of warm dense gold. The ac conductivity can be described by the Drude model,

$$\sigma(\omega)=\frac{\sigma_0}{1+(\omega\tau)^2}, \tag{3}$$

where τ is the collisional relaxation time. This formula has been used to fit the low-frequency part of the QMD frequency-dependent conductivities for the four considered temperatures shown in Fig. 4. As the static conductivity σ_0 is taken from the QMD results, this fitting procedure allows us to determine a collisional relaxation time τ_D and an electron

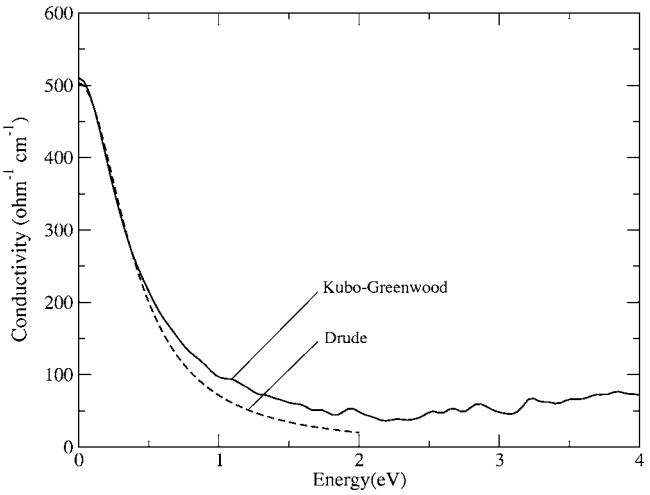

FIG. 5. Frequency-dependent conductivity for gold at $\rho=0.5$ g/cm^3 and $T=30\,000$ K.

density n_{eD} from $n_{eD}=m_e\sigma_0/\tau_D/e^2$, where m_e is the electron mass. As an illustration, the result of one such fit is shown in Fig. 5 for a temperature of 30 000 K. The agreement between the Lorentzian fit and the QMD simulations is correct at low energy where there are no interband transitions. The collisional relaxation time and the mean ionization Z_D obtained from this fitting procedure are displayed in Table II.

The mean ionization Z_D inferred from the Drude model, assuming NFE behavior of warm dense gold, is the first of three different estimations of the mean ionization that we obtained from QMD simulations. Two other methods were used to define a representative value of the number of free electrons. Such estimations provide a useful metric and can be used to compare and validate the electronic structure calculated by the various plasma models. In the second method, the number of electrons having their energy level beyond the Fermi energy is calculated using Fermi-Dirac occupations. The results are noted Z_{FL} in Table II. In the third method, we used an ideal plasma model assuming that (i) we can separate the thermodynamics functions of ions and electrons; (ii) the ions form an ideal gas; and (iii) the electrons form a free-electron gas without interactions. The validity of each of these assumptions in the low-temperature and intermediate density regime studied here is questionable. Nevertheless, such model provide a simple and useful metric knowing the total pressure of the plasma. By subtracting the pressure of the ideal gas from the QMD pressure, an electronic contribution to the pressure is obtained from which we extract a mean ionization, noted Z_{IP} in Table II. The last column displayed in Table II is the TFD mean ionization Z_{TFD}. In this intermediate density regime, the TFD mean ionization is 3 times greater than Z_D at 15 000 K and 1.4 times greater at 30 000 K. The three criteria lead to three different values of the mean ionization, and the difference between these three values and the TFD mean ionization reduces when the temperature increases.

The difference between the inferred mean ionizations shows that an accurate calculation of the local electronic structure of WDM is still a theoretical challenge. Despite mean ionization being key data to calculate transport properties in dense plasmas, there is no unequivocal definition for it. QMD calculations overcome this disability and allow a direct determination of transport coefficients, such as thermal conductivity [33]. Furthermore, by providing an accurate self-consistent set of transport coefficients and thermodynamic data, QMD simulations could be used to benchmark the various plasma statistical physics models in the WDM regime.

V. CONCLUSION

To summarize, we have carried out an experiment measuring directly electrical resistivity, pressure, and internal energy variation of gold plasmas at a density of $\rho=0.5$ g/cm^3 in the internal energy range 8–12 MJ/kg. In this thermodynamic regime, close to the saturation curve and in the vicinity of the metal-insulator transition, QMD simulations are in good agreement with the experimental equation of state data as well as the electrical resistivity for temperatures ranging from 15 000 to 30 000 K. These comparisons demonstrate the capabilities of QMD simulations to accurately calculate the constituency of warm dense gold and also the various density effects. The behavior of the calculated frequency-dependent conductivities shows a clear dependence with the temperature. An important contribution of the $6s\rightarrow 6p$ and $5d\rightarrow 6p$ transitions is observed as well as an increase of the free-free transitions, i.e., a Drude form, when the temperature is increasing. Different estimations of the mean ionization were obtained from different physical criteria, leading to different value of this quantity. Such study illustrates the problem of the mean ionization calculation in dense plasma

TABLE II. Temperature T, electrical conductivity σ_0 as given by the Kubo-Greenwood formula, collisional relaxation time τ_D, and mean ionization Z_D, deduced from the Drude fit of the low-frequency part of the calculated frequency-dependent conductivity, mean ionization Z_{IP} deduced from the ideal plasma model, mean ionization Z_{FL} from the fraction of electrons having their energy level beyond the Fermi level, and TFD mean ionization Z_{TFD}.

T (K)	σ_0 ($[\Omega\ \mathrm{m}]^{-1}$)	τ_D (fs)	Z_D	Z_{IP}	Z_{FL}	Z_{TFD}
15 000	9 800	1.50	0.15	0.05	0.29	0.46
20 000	23 800	1.72	0.32	0.16	0.61	0.66
25 000	38 100	1.68	0.53	0.37	0.97	0.85
30 000	50 300	1.62	0.72	0.54	1.24	1.02

models. This latter point is at the heart of the difficulty in calculating transport and thermodynamic properties along the transition into the WDM regime using standard plasma statistical physics models. We showed that QMD simulations should be used to validate such models by providing an accurate self-consistent set of transport coefficients and thermodynamic data.

ACKNOWLEDGMENTS

It is a pleasure to thank B. Loffredo and M. Sonnaert for their technical assistance during the course of this work. We also thank F. Lambert for making the results of the TFD code available.

[1] S. Ichimaru, *Statistical Plasma Physics, Vol. II: Condensed Plasmas* (Addison-Wesley, New York, 1994).
[2] F. Perrot and M. W. C. Dharma-wardana, Phys. Rev. E **52**, 5352 (1995).
[3] V. Recoules, P. Renaudin, J. Clérouin, P. Noiret, and G. Zérah, Phys. Rev. E **66**, 056412 (2002).
[4] M. P. Desjarlais, J. D. Kress, and L. A. Collins, Phys. Rev. E **66**, 025401(R) (2002).
[5] C. Blancard and G. Faussurier, Phys. Rev. E **69**, 016409 (2004).
[6] J. F. Benage, Phys. Plasmas **7**, 2040 (2000), and references therein.
[7] V. N. Korobenko, A. D. Rakhel, A. I. Savvatimski, and V. E. Fortov, Phys. Rev. B **71**, 014208 (2005).
[8] A. Ng, D. Parfeniuk, P. Celliers, L. DaSilva, R. M. More, and Y. T. Lee, Phys. Rev. Lett. **57**, 1595 (1986).
[9] A. Ng, P. Celliers, A. Forsman, R. M. More, Y. T. Lee, F. Perrot, M. W. C. Dharma-wardana, and G. A. Rinker, Phys. Rev. Lett. **72**, 3351 (1994).
[10] A. N. Mostovych and Y. Chan, Phys. Rev. Lett. **79**, 5094 (1997).
[11] H. Yoneda, H. Morikami, K. I. Ueda, and R. M. More, Phys. Rev. Lett. **91**, 075004 (2003); H. Morikami, H. Yoneda, K. I. Ueda, and R. M. More, Phys. Rev. E **70**, 035401(R) (2004).
[12] K. Widmann, T. Ao, M. E. Foord, D. F. Price, A. D. Ellis, P. T. Springer, and A. Ng, Phys. Rev. Lett. **92**, 125002 (2004).
[13] P. Audebert, P. Renaudin, S. Bastiani-Ceccotti, J.-P. Geindre, C. Chenais-Popovics, S. Tzortzakis, V. Nagels-Silvert, R. Shepherd, I. Matsushima, S. Gary, F. Girard, O. Peyrusse, and J.-C. Gauthier, Phys. Rev. Lett. **94**, 025004 (2005).
[14] P. Renaudin, C. Blancard, G. Faussurier, and P. Noiret, Phys. Rev. Lett. **88**, 215001 (2002).
[15] P. Renaudin, C. Blancard, J. Clérouin, G. Faussurier, P. Noiret, and V. Recoules, Phys. Rev. Lett. **91**, 075002 (2003).
[16] J. C. Jamieson, J. N. Fritz, and M. H. Manghnani, in *High-Pressure Research in Geophysics*, edited by S. Akimoto and M. H. Manghnani (Center for Academic Publishing, Tokyo, 1982), p. 27.
[17] P. Drude, Ann. Phys. **1**, 566 (1900).
[18] D. Mermin, Phys. Rev. **137**, A1441 (1965).
[19] D. M. Ceperley and B. J. Alder, Phys. Rev. Lett. **45**, 566 (1980).
[20] P. E. Blöchl, Phys. Rev. B **50**, 17953 (1994).
[21] G. Kresse and D. Joubert, Phys. Rev. B **59**, 1758 (1999).
[22] H. J. Monkhorst and J. D. Pack, Phys. Rev. B **13**, 5188 (1976).
[23] J. E. Peralta, J. Uddin, and G. E. Scuseria, J. Chem. Phys. **122**, 084108 (2005).
[24] J. C. Boettger, Phys. Rev. B **67**, 174107 (2003).
[25] R. Ahuja, S. Rekhi, and B. Johansson, Phys. Rev. B **63**, 212101 (2001).
[26] J. M. Soler, M. R. Beltran, K. Michaelian, I. L. Garzon, P. Ordejon, D. Sanchez-Portal, and E. Artacho, Phys. Rev. B **61**, 5771 (2000).
[27] T. Tsuchiya and K. Kawamura, J. Chem. Phys. **116**, 2121 (2002).
[28] G. Kresse and J. Hafner, Phys. Rev. B **47**, R558 (1993); G. Kresse and J. Furthmuller, Comput. Mater. Sci. **6**, 15 (1996); Phys. Rev. B **54**, 11169 (1996).
[29] R. Kubo, J. Phys. Soc. Jpn. **12**, 570 (1957).
[30] D. A. Greenwood, Proc. Phys. Soc. London **71**, 585 (1958).
[31] S. Mazevet, M. P. Desjarlais, L. A. Collins, J. D. Kress, and N. H. Magee, Phys. Rev. E **71**, 016409 (2005).
[32] J. Clérouin, P. Renaudin, Y. Laudernet, P. Noiret, and M. P. Desjarlais, Phys. Rev. B **71**, 064203 (2005).
[33] V. Recoules and J.-P. Crocombette, Phys. Rev. B **72**, 104202 (2005).